Real-space imaging of interfacial water with submolecular resolution

Jing Guo[1,2][†], Xiangzhi Meng[1,2][†], Ji Chen[1,2][†], Jinbo Peng[1,2], Jiming Sheng[1,2], Xin-Zheng Li[1,2], Limei Xu[1,2], Jun-Ren Shi[1,2], Enge Wang[1,2]★ and Ying Jiang[1,2]★

Water/solid interfaces are vital to our daily lives and are also a central theme across an incredibly wide range of scientific disciplines. Resolving the internal structure, that is, the O–H directionality, of water molecules adsorbed on solid surfaces has been one of the key issues of water science yet it remains challenging. Using a low-temperature scanning tunnelling microscope, we report submolecular-resolution imaging of individual water monomers and tetramers on NaCl(001) films supported by a Au(111) substrate at 5 K. The frontier molecular orbitals of adsorbed water were directly visualized, which allowed discrimination of the orientation of the monomers and the hydrogen-bond directionality of the tetramers in real space. Comparison with *ab initio* density functional theory calculations reveals that the ability to access the orbital structures of water stems from the electronic decoupling effect provided by the NaCl films and the precisely tunable tip–water coupling.

Water/solid interfaces are ubiquitous and play a crucial role across a broad spectrum of materials science such as heterogeneous catalysis, photoconversion, electrochemistry, sensors, electronic devices, corrosion and lubrication[1,2]. One of the most fundamental issues in all of these applied fields is the characterization of hydrogen-bonded networks formed on surfaces[3–5] and hydrogen-atom transfer through hydrogen bonds[6,7], which are responsible for many extraordinary physical and chemical properties of water/solid interfaces. Ideally, attacking this problem requires access to the internal degrees of freedom of water molecules, that is, the directionality of OH bonds, which still remains a great challenge owing to the light mass and small size of hydrogen. So far, spectroscopic techniques have been employed to identify the bond orientation of interfacial water molecules through vibrational fingerprints. However, all of these techniques suffer from a lack of spatial resolution and the difficulty of spectral assignment[8,9].

Orbital imaging is a promising technique for resolving in real space the O–H directionality of interfacial water, because molecular orbitals are spatially locked together with the geometric structures of molecules. The scanning tunnelling microscope (STM) has proved to be ideal for selectively imaging the molecular orbitals with submolecular resolution[10]. However, it has not been possible so far to access the internal orbital structures of water with STM despite massive efforts in the past decade and individual water molecules are usually imaged as featureless round protrusions[11–21]. This is mainly because most of the STM studies on water were restricted to metal surfaces, which led to significant broadening and distortion of the molecular orbitals of water because of coupling to the electronic states of the metallic substrates. In addition, the frontier orbitals of adsorbed water are usually located far away from the Fermi level (E_F), thus probing the orbitals through resonant tunnelling is prohibited owing to the instability of water under large bias voltages[18].

Here, we demonstrate unprecedented submolecular imaging of water on a Au-supported insulating NaCl(001) film, a system

of great importance to environmental and biological sciences regarding salt dissolution, salt-catalysed ice nucleation, and heterogeneous chemical reactions[22–24]. The NaCl film decouples water molecules electronically from the Au substrate such that the native molecular orbitals of water are mostly preserved. A STM tip is employed as a nano-substrate to enhance the molecular density of states (DOS) near E_F through tunable tip–water coupling, which facilitates direct imaging of lowest unoccupied (LUMO) and highest occupied (HOMO) molecular orbitals of water at small bias voltages. Furthermore, we show the possibility of discerning the orientation of water monomers and the hydrogen-bond directionality of water tetramers through submolecular-resolution orbital imaging.

On deposition on Au(111) at room temperature, NaCl forms bilayer (001)-terminated islands with perfect nonpolar step edges[25]. The NaCl prefers to nucleate at step edges of the Au(111) surface and follows a carpet-like growth mode over the steps (Fig. 1a). The square lattice of Cl⁻ anions is clearly resolved in the high-resolution STM image (Fig. 1b). The Na⁺ cations shown in the molecular model of the NaCl(001) surface (Fig. 1c) are invisible in Fig. 1b because the highest DOS around the Fermi edge coincides with the sites of Cl⁻ (ref. 26). The nearest-neighbour distance between two Cl⁻ is about 3.90 ± 0.05 Å, very close to that of bulk NaCl ($\sim$3.99 Å). The tail of electron density from Au(111) that extends through the NaCl layers facilitates the tunnelling process and enables the imaging of water on the NaCl islands.

Water forms isolated monomers on the NaCl islands at 5 K (Fig. 1d). The water monomer exhibits an interesting double-lobe structure with two orthogonal orientations (Fig. 1e,f). With the underlying Cl⁻ sub-lattice superimposed, we found that the monomer was bonded on top of Na⁺ and aligned with the Na⁺–Cl⁻ direction. *Ab initio* calculations based on the density functional theory (DFT) with Van der Waals corrections reveal that the molecular plane of water is perpendicular to the surface as shown in Fig. 1g,h. One OH bond points laterally towards the neighbouring Cl⁻ and the other points upward away from the surface. Long-range dispersion forces from the Au substrate stabilize such a 'standing'

[1]International Center for Quantum Materials (ICQM) and School of Physics, Peking University, Beijing 100871, China, [2]Collaborative Innovation Center of Quantum Matter, Beijing, China. [†]These authors contributed equally to this work. *e-mail: egwang@pku.edu.cn; yjiang@pku.edu.cn
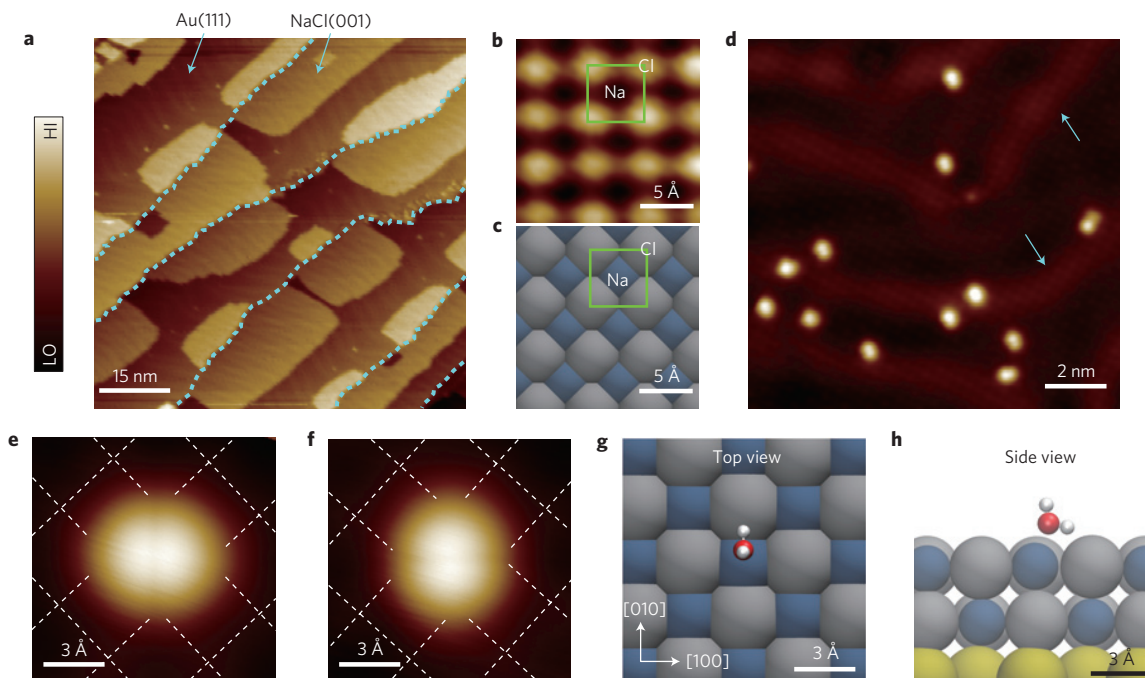
Figure 1 | Water monomers adsorbed on NaCl(001)/Au(111). a, STM topography of bilayer NaCl(001) islands grown on the Au(111) surface. Step edges of the Au(111) surface are highlighted by blue dotted lines. Set point: $V = 2.0$ V and $I = 9$ pA. **b**, Atomically resolved STM image on a NaCl(001) island. Only the anions Cl$^-$ are imaged as protrusions. Set point: $V = 50$ mV and $I = 20$ pA. **c**, Molecular model of the NaCl(001) surface. The unit cells are highlighted by green squares in **b,c**. **d**, Zoom-in STM topography of a NaCl(001) island after dosing about 0.01 bilayer of water molecules at 5 K. The single protrusions correspond to individual water monomers. Herringbone structures of the underlying Au(111) substrate are denoted by blue arrows. Set point: $V = 100$ mV and $I = 50$ pA. **e,f**, STM images of two water monomers with orthogonal orientations. Square lattices of the NaCl(001) surface arising from Cl$^-$ are depicted by white grids. Set point: $V = 100$ mV and $I = 50$ pA. **g,h**, Top (**g**) and side (**h**) views of the calculated adsorption configuration of a water monomer. O, H, Au, Cl$^-$ and Na$^+$ are denoted by red, white, gold, grey and dark-cyan spheres, respectively.
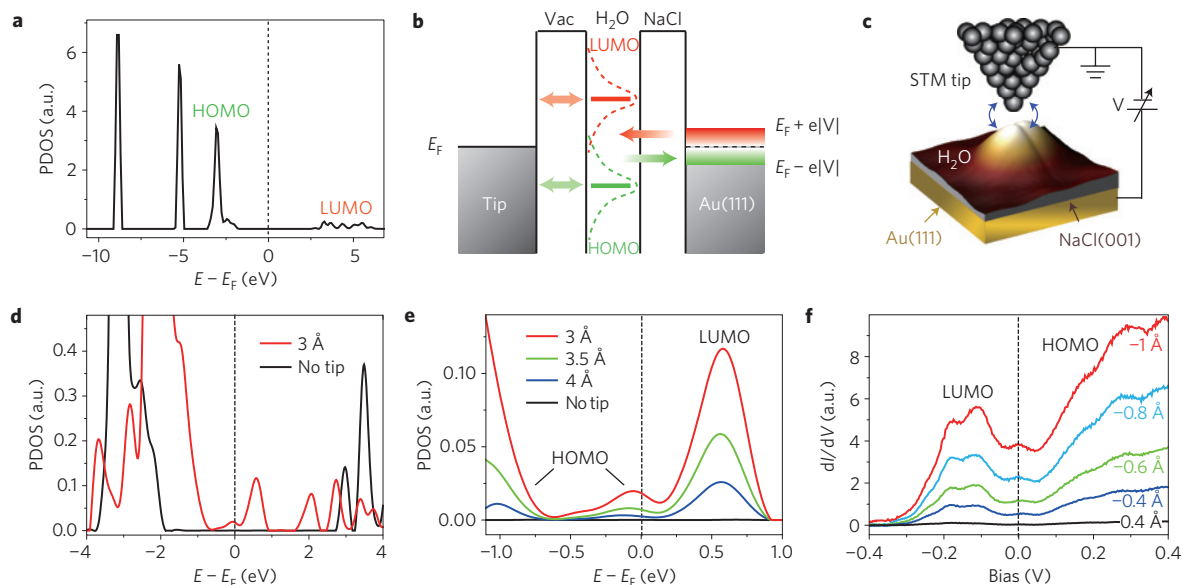

Figure 2 | Development of the HOMO and LUMO states of a water monomer near the Fermi level due to tip–water coupling. a, PDOS projected onto the water molecule for a water monomer adsorbed on NaCl(001). The energy zero is the Fermi level. **b**, Schematic of a double-barrier single-molecule junction of water. The coupling of the HOMO and LUMO with the tip is denoted by double-ended green and red arrows, respectively, leading to a Lorentzian-shape broadening of HOMO (dashed green line) and LUMO (dashed red line). The single-ended green and red arrows denote the flowing directions of tunnelling currents at the positive and negative biases, respectively. **c**, Schematic of the experimental STM set-up corresponding to **b**, in which the tip–water coupling is denoted by double-ended blue arrows. **d**, Calculated PDOS of a water monomer without and with tip–water coupling. The tip–water separation is 3 Å, which is defined as the vertical distance between the endmost atom of the STM tip and the oxygen atom of water. **e**, Zoom-in PDOS near E_F at different tip–water separations. **f**, dI/dV spectra of a water monomer measured at different tip heights (z). Z offsets are referenced to the gap set with: $V = 100$ mV and $I = 50$ pA.

adsorption configuration against the flat ones reported previously (for details, see Supplementary Fig. 1 and Table 1)[27,28].

The calculated projected DOS (PDOS) for water/NaCl(001)/Au(111) shows that the E_F falls into the HOMO–LUMO gap of the water monomer (Fig. 2a). Owing to the electronic decoupling effect provided by the NaCl film, the broadenings of the HOMO and LUMO arising from coupling to the electronic states of the Au substrate are very small, resulting in negligible molecular DOS within the energy range from −2 to 2 eV. It should be noted that for imaging of small molecules such as water one has to use small bias voltages (typically dozens of millivolts) to avoid the instability induced by inelastic electrons[29]. In such a case, electrons from the tip should tunnel directly into the Au(111) substrate and no orbital structures of water can be probed, unless there exist other mechanisms bringing about the development of HOMO and LUMO states near E_F.

It is known that the STM tip not only acts as a probe, but may modify the molecular DOS around E_F through tip–molecule coupling[30] (Fig. 2b,c). The calculated PDOS (Fig. 2d) of a water monomer with a tip–water separation of 3 Å exhibits considerable broadenings and shifts of the HOMO and LUMO towards E_F because of coupling to the continuum of tip states in agreement with the Newns–Anderson model[31]. There is no signature of appreciable covalent coupling between the tip and the HOMO/LUMO. Figure 2e shows the zoom-in PDOS near E_F with the tip–water separation changing from 3 to 4 Å. It is worth noting that the molecular DOS is already quite prominent near the E_F at a tip–water separation of 4 Å. The tail states below −0.5 eV and the ones at E_F are mostly of HOMO character whereas the states around 0.6 eV are mostly of LUMO character, as determined from inspection of the real-space distribution of the charge density within corresponding energy windows. As the tip approaches the monomer, both the HOMO- and LUMO-like states near E_F are enhanced owing to the increased tip–water coupling.

For comparison, we measured dI/dV spectra at different tip heights (Fig. 2f). The background signals arising from the direct tunnelling between the tip and the Au substrate were removed from the original dI/dV spectra (see Supplementary Fig. 3 and related discussion for more details). In qualitative agreement with the calculated PDOS (Fig. 2e), the dI/dV curves exhibit a tail feature developed from the positive bias and a broad peak around −0.15 V, which are, respectively, attributed to the HOMO and LUMO states from the bias-dependent orbital images (see below). The magnitudes of those states increase as the tip height decreases. The discrepancy of the energy scale between the dI/dV spectra and the PDOS may result from the uncertainty of the tip apex (see Supplementary Figs 4–5). Another possible origin is the non-local electron interaction with image charges in the tip, which may induce additional shifts of the HOMO/LUMO levels towards E_F (ref. 32).

For the STM set-up shown in Fig. 2c where the bias voltage is applied to the sample, one would expect to probe the HOMO at negative biases and the LUMO at positive biases. However, this is true only when the tip–water interaction is negligible. In our case, the tip–water coupling is significantly stronger than the water–substrate (Au) coupling owing to the electronic decoupling effect provided by the NaCl film, such that the molecular states of the adsorbed water are pinned to the E_F of the STM tip instead of the Au substrate when the bias is applied (Fig. 2b). Thus, the tip could be considered as a 'nano-substrate' and the Au substrate becomes a macroscopic 'tip', leading to observations of the HOMO at positive biases and the LUMO at negative biases (Fig. 2f). Although the tip–water coupling is strong enough to modify the molecular DOS of water, the highly hydrophilic nature of the NaCl(001) surface ensures that the water molecules can remain stable on the substrate in the presence of tip–water coupling (see Supplementary Fig. 7).
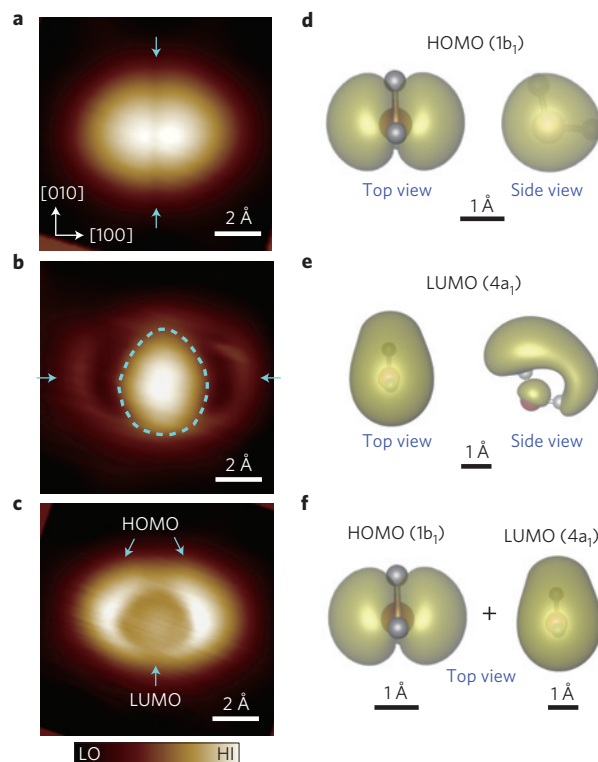

Figure 3 | Orbital imaging of a water monomer with submolecular resolution. a–c, High-resolution STM images of HOMO (**a**), LUMO (**b**) and HOMO+LUMO (**c**) of a water monomer. Set point: $V = 100$ mV and $I = 500$ pA (**a**); $V = −100$ mV and $I = 800$ pA (**b**); $V = −50$ mV and $I = 550$ pA (**c**). **d–f,** Calculated molecular orbitals of a water monomer adsorbed on NaCl(001) by plotting isosurfaces of charge densities integrated over 1 eV of the HOMO/LUMO tail close to E_F. O and H atoms of H_2O are denoted by red and light-grey spheres, respectively. The arrows in **a** indicate the nodal plane of the HOMO. The dashed oval and arrows in **b** highlight the egg shape of the LUMO and the faint ring structures arising from the remaining HOMO, respectively. The arrows in **c** highlight that the development of the LUMO deviates from the centre towards the lower edge of the HOMO.

Now we show the possibility of selectively imaging the frontier molecular orbitals of water in real space. Figure 3a shows a typical STM image taken at a positive bias voltage within the tail region of the dI/dV spectra in Fig. 2f. The observed double-lobe structure agrees perfectly with the calculated HOMO ($1b_1$) of an adsorbed monomer (Fig. 3d). The mirror symmetry of the two lobes with respect to the nodal plane (highlighted by arrows in Fig. 3a) confirms that the HOH plane of water is perpendicular to the surface. When changing to a negative bias voltage corresponding to the peak position in Fig. 2f, the double-lobe structure almost fades out and an egg-shaped lobe appears within the nodal plane of the HOMO (highlighted by a dashed oval in Fig. 3b), very closely resembling the LUMO ($4a_1$) of the monomer (Fig. 3e). The egg-shaped LUMO lobe, with only one axis of symmetry, allows us to determine that the flat OH bond of the monomer is oriented along the [010] direction of the NaCl(001) surface.

We note that there still exists a tiny contribution from the HOMO in Fig. 3b, which appears as two faint ring structures (denoted by arrows in Fig. 3b). By choosing appropriate bias voltages, it is possible to tune the relative contributions from the HOMO and LUMO. Figure 3c shows such a composite STM image in which the HOMO and LUMO can be probed simultaneously with comparable contributions. Interestingly, the LUMO feature does not develop from the centre but towards the lower edge of
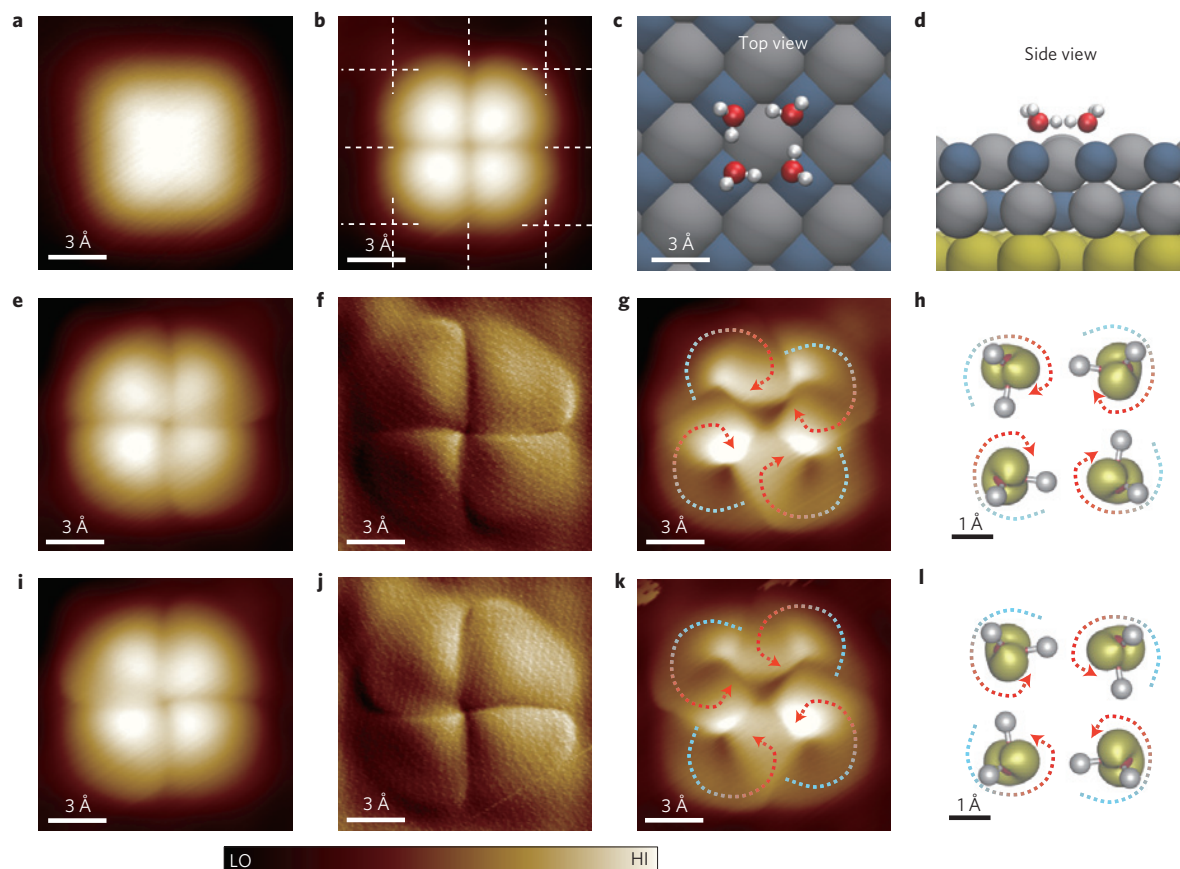
Figure 4 | Adsorption configuration and orbital imaging of water tetramers on NaCl(001)/Au(111). a,b, STM images of a water tetramer acquired at different tunnelling gaps. The white square grid in **b** denotes the sub-lattice of Cl^-. Set point: $V = 40$ mV and $I = 10$ pA (**a**); $V = 10$ mV and $I = 50$ pA (**b**). **c,d**, Top (**c**) and side (**d**) views of the calculated adsorption configuration of a tetramer. **e–l**, HOMO imaging and calculations of two degenerate chiral water tetramers with anticlockwise (**e–h**) and clockwise (**i–l**) hydrogen-bonded loops. **e,i**, STM images of the water tetramers. Set point: $V = 10$ mV and $I = 80$ pA. **f,j**, Derivative images of **e,i**, respectively. **g,k**, STM images of the water tetramers with enhanced tip–water coupling. Set point: $V = 10$ mV and $I = 140$ pA. The lobes of the water tetramers shown in **e,i** are resolved into helical structures as highlighted by curved dotted arrows with gradient (high, red; low, blue). **h,l**, Calculated HOMO of the two chiral tetramers by plotting isosurfaces of charge densities integrated over 1 eV of the HOMO tail close to E_F. The chirality of the HOMO resembles that of the helical structures as shown in **g,k**.

the HOMO (see arrows in Fig. 3c). This deviation implicates the directionality of the upright OH of the monomer, which is not strictly vertical but slightly tilts away from the surface normal towards the [0$\bar{1}$0] direction (Fig. 1g,h).

To obtain more comprehensive information, we measured orbital images of a water monomer by varying the bias voltage and the tunnelling current in a systematic way (Supplementary Fig. 8), from which three main features can be extracted: the HOMO and LUMO features only emerge at small tip heights and become prominent as the tip height decreases; the HOMO gradually evolves into the LUMO when the polarity of the bias voltage changes from positive to negative; the images acquired around zero bias voltages are dominantly contributed by the HOMO, whereas the LUMO becomes overwhelming when the bias voltage drops below −100 mV. Different STM tips yield similar HOMO and LUMO features in spite of the variation in the energy scale and the selective sensitivity to HOMO or LUMO orbitals (see Supplementary Fig. 6). It is worth noting that such HOMO/LUMO imaging also allows us to discern the orientation of asymmetric monomers whose molecular planes are not perpendicular to the surface (see Supplementary Fig. 9).

It is striking that the measured orbital images in the presence of the tip–water coupling reflect essentially the unperturbed molecular orbitals of water on NaCl(001) (Fig. 3). DFT calculations reveal that the spatial orbital structure of the water monomer barely changes

for tip–water separation above 3 Å. It is not until the tip–water separation gets too small (possibly <3 Å) that the orbital shape of water could be changed or distorted owing to the covalent coupling between the tip and water as shown in Supplementary Figs 10 and 11. Therefore, it is important in the experiments to carefully tune the tip height into an optimal range, where the influence of the tip on the original adsorption configuration and the orbital shape of water is negligible while the molecular DOS around the E_F enhanced by the tip–water coupling is still sufficient for high-resolution orbital imaging.

Figure 2e,f shows considerable overlaps of the HOMO and LUMO around E_F, which facilitates the simultaneous imaging of the HOMO and LUMO as shown in Fig. 3c. It is worth noting that the composite STM image (Fig. 3c) does not correspond to a simple superposition of the HOMO and LUMO (Fig. 3f). The discrepancy might arise from the interference effect between the tunnelling paths through the two orbitals. Although the overall resemblance of the STM images with the orbitals of the unperturbed water molecule is directly evident, more accurate simulation of the STM images requires full calculation of the tip–water–surface system such as elastic scattering quantum chemistry calculations[33], especially when multiple tunnelling channels are involved.

In the following we apply the orbital-imaging technique to water tetramers, which are constructed by manipulating individual water monomers with the STM tip as demonstrated in Supplementary

Fig. 12. The water tetramer appears as a featureless square protrusion with a flat top at a large tip–molecule separation (Fig. 4a), which splits into four equivalent lobes as the tip height decreases (Fig. 4b). The geometric centre of the tetramer is right above the Cl^- with the four water molecules adsorbed on the Na^+ (Fig. 4b). The calculated most stable tetramer structure is shown in Fig. 4c,d (for more details, see Supplementary Fig. 2 and Table 2). Each water molecule donates and accepts just one hydrogen bond yielding a cyclic tetramer. The other four free OH bonds point obliquely upward away from the surface. The observed flat tetramer is more stable than the buckled one predicted in ref. 28.

Interestingly, we note that such a tetramer structure contains two degenerate chiral states: clockwise and anticlockwise hydrogen-bonded loops. To the best of our knowledge, it has not been possible to distinguish the directionality of hydrogen-bonded networks of water clusters[34]. It was found that the tip–water coupling shifts and broadens the HOMO states over E_F, whereas the LUMO states are less affected and stay well above E_F (see Supplementary Fig. 13 and related discussion). After switching on the tip–water coupling, the four lobes of the tetramer become no longer equivalent but slightly distorted, such that the boundaries between the four lobes exhibit left-handed (Fig. 4e) or right-handed (Fig. 4i) rotation. The chirality of the tetramer is more evident in the corresponding derivative images (Fig. 4f,j).

Further increasing the tip–water coupling, each lobe of the tetramer is resolved into a striking helical structure (Fig. 4g,k). The apparent height of the observed structure increases helically as denoted by curved dotted arrows in Fig. 4g,k, resulting in remarkable chirality. Such helical structures correlate well with the calculated isosurfaces of the charge densities of the HOMO (Fig. 4h,l), which exhibit similar chirality due to the tilt of the HOH plane from the surface normal. Comparison between the orbital images and the HOMO isosurfaces allows us to identify the directionality of hydrogen bonds and the orientation of free OH bonds in different water tetramers.

These results not only shed new light on the microscopic understanding of water adsorption on salts, but also open up the possibility of determining the detailed topology of hydrogen-bonded networks at water/solid interfaces with atomic precision. The ability to discern the O–H directionality of water provides further opportunities for probing the dynamics of hydrogen-bonded networks at the atomic scale such as hydrogen-atom transfer and bond rearrangement. Furthermore, the orbital-imaging technique assisted by the tunable tip–molecule coupling reveals a new understanding of STM experiments, which is crucial for high-resolution imaging in a broad range of molecular systems and materials.

Methods

Experimental. The experiments were performed with an ultrahigh-vacuum cryogenic (5 K) STM (Createc) with the base pressure better than 5×10^{-11} torr. The Au(111) single crystal was repeatedly sputtered with argon and annealed at about 900 K, until a clean Au(111)-22 $\times \sqrt{3}$ reconstructed surface was obtained. The NaCl (Sigma Aldrich, 99.999%) was then evaporated thermally from a Knudsen cell at a temperature of 720 K onto the Au(111) surface held at room temperature. The ultrapure H_2O (Sigma Aldrich, deuterium-depleted) was further purified under vacuum by freeze–thaw cycles to remove remaining impurities. The H_2O molecules were dosed *in situ* onto the sample surface at 5 K with a rate of 0.01 bilayer min^{-1} through a dosing tube, which pointed towards the sample from a distance of about 6 cm. The subsequent STM measurements were all performed at 5 K with electrochemically etched tungsten tips, which were cleaned by alternative annealing and sputtering before the experiments, and further by controlled field-emission and tip-crash procedures during the scanning. Bias voltage refers to the sample voltage with respect to the tip. All of the STM topographic images were obtained in constant-current mode. The scanning tunnelling spectroscopy dI/dV spectra were acquired using lock-in detection of the tunnelling current by adding a 10 mV_{rms} modulation at 250 Hz to the sample bias. Image processing was performed by Nanotec WSxM (ref. 35).

Theoretical. DFT calculations were performed to study the adsorption of water monomers and tetramers on a NaCl(001) surface. Van der Waals corrections for dispersion forces were considered within the vdW-DF scheme using the optB88-vdW method[36] as implemented in the Vienna *ab initio* simulation package[37,38]. Projector augmented-wave pseudopotentials[39] were used together with a plane-wave basis set and a cutoff energy of 550 eV for the expansion of the electronic wavefunctions. To include the Au(111) substrate in the DFT calculation, we constructed a coincidence structure by superposing a NaCl (2 × 2) unit cell on a $\begin{pmatrix} 3 & 1 \\ 1 & 3 \end{pmatrix}$ superstructure of the Au(111) H-bonded substrate with a residual strain of about 5% (ref. 25). To match the square symmetry of the NaCl(001) lattice, the angle of the $\begin{pmatrix} 3 & 1 \\ 1 & 3 \end{pmatrix}$ supercell of the Au(111) substrate was changed from 82° to 90°. The Au substrate was modelled by a four-layer slab. A bilayer NaCl(001) slab with a lattice constant of 5.665 Å was used according to the experimental condition. The bottom layer of the NaCl and the Au substrate were fixed during geometry relaxations. The Brillouin zone was sampled using a (2 × 2 × 1) Monkhorst–Pack k-point mesh. Considering that the STM tip was repeatedly indented into the Au sample for tip shaping in the experiment and thus most likely coated with gold, the STM tip was constructed using Au atoms with different apices for comparison (for details, see Supplementary Fig. 4). No matter whether the tip atoms were fixed or not during the relaxation, the calculation results were barely affected as long as the tip–water separation was larger than 3 Å. The diffusion barrier of a water monomer on a NaCl(001) surface and the energy barriers between different adsorption configurations of water monomers were calculated using the nudged elastic band method[40].

References

1. Henderson, M. A. Redox properties of water on the oxidized and reduced surfaces of CeO$_2$(111). *Surf. Sci. Rep.* **46,** 1–308 (2002).
2. Hodgson, A. & Haq, S. Water adsorption and the wetting of metal surfaces. *Surf. Sci. Rep.* **64,** 381–451 (2009).
3. Feibelman, P. J. Partial dissociation of water on Ru(0001). *Science* **295,** 99–102 (2002).
4. Meng, S., Xu, L. F., Wang, E. G. & Gao, S. Vibrational recognition of hydrogen-bonded water networks on a metal surface. *Phys. Rev. Lett.* **89,** 176104 (2002).
5. Carrasco, J., Hodgson, A. & Michaelides, A. A molecular perspective of water at metal interfaces. *Nature Mater.* **11,** 667–674 (2012).
6. Nagasaka, M., Kondoh, H., Amemiya, K., Ohta, T. & Iwasawa, Y. Proton transfer in a two-dimensional hydrogen-bonding network: Water and hydroxyl on a Pt(111) surface. *Phys. Rev. Lett.* **100,** 106101 (2008).
7. Kumagai, T., Okuyama, H., Hatta, S., Aruga, T. & Hamada, I. H-atom relay reactions in real space. *Nature Mater.* **11,** 167–172 (2012).
8. Shen, Y. R. & Ostroverkhov, V. Sum-frequency vibrational spectroscopy on water interfaces: Polar orientation of water molecules at interfaces. *Chem. Rev.* **106,** 1140–1154 (2006).
9. Kimmel, G. A. *et al.* Polarization- and azimuth-resolved infrared spectroscopy of water on TiO$_2$(110): Anisotropy and the hydrogen-bonding network. *J. Phys. Chem. Lett.* **3,** 778–784 (2012).
10. Repp, J., Meyer, G., Stojković, S. M., Gourdon, A. & Joachim, C. Molecules on insulating films: Scanning-tunneling microscopy imaging of individual molecular orbitals. *Phys. Rev. Lett.* **94,** 026803 (2005).
11. Mitsui, T., Rose, M. K., Fomin, E., Ogletree, D. F. & Salmeron, M. Water diffusion and clustering on Pd(111). *Science* **297,** 1850–1852 (2002).
12. Morgenstern, K. & Nieminen, J. Intermolecular bond length of ice on Ag(111). *Phys. Rev. Lett.* **88,** 066102 (2002).
13. Cerdá, J. *et al.* Novel water overlayer growth on Pd(111) characterized with scanning tunneling microscopy and density functional theory. *Phys. Rev. Lett.* **93,** 116101 (2004).
14. Verdaguer, A., Sacha, G. M., Bluhm, H. & Salmeron, M. Molecular structure of water at interfaces: Wetting at the nanometer scale. *Chem. Rev.* **106,** 1478–1510 (2006).
15. Michaelides, A. & Morgenstern, K. Ice nanoclusters at hydrophobic metal surfaces. *Nature Mater.* **6,** 597–601 (2007).
16. Carrasco, J. *et al.* A one-dimensional ice structure built from pentagons. *Nature Mater.* **8,** 427–431 (2009).
17. He, Y., Tilocca, A., Dulub, O., Selloni, A. & Diebold, U. Local ordering and electronic signatures of submonolayer water on anatase TiO$_2$(101). *Nature Mater.* **8,** 585–589 (2009).
18. Shin, H-J. *et al.* State-selective dissociation of a single water molecule on an ultrathin MgO film. *Nature Mater.* **9,** 442–447 (2010).
19. Hammer, B., Wendt, S. & Besenbacher, F. Water adsorption on TiO$_2$. *Top. Catal.* **53,** 423–430 (2010).
20. Nie, S., Feibelman, P. J., Bartelt, N. C. & Thürmer, K. Pentagons and heptagons in the first water layer on Pt(111). *Phys. Rev. Lett.* **105,** 026102 (2010).

21. Okuyama, H. & Hamada, I. Hydrogen-bond imaging and engineering with a scanning tunnelling microscope. *J. Phys. D* **44,** 464004 (2011).
22. Allen, H. C., Laux, J. M., Vogt, R., Finlayson-Pitts, B. J. & Hemminger, J. C. Water-induced reorganization of ultrathin nitrate films on NaCl: Implications for the tropospheric chemistry of sea salt particles. *J. Phys. Chem.* **100,** 6371 (1996).
23. Taylor, D. P., Hess, W. P. & McCarthy, M. I. Structure and energetics of the water/NaCl(100) interface. *J. Phys. Chem. B* **101,** 7455–7463 (1997).
24. Liu, L. M., Laio, A. & Michaelides, A. Initial stages of salt crystal dissolution determined with *ab initio* molecular dynamics. *Phys. Chem. Chem. Phys.* **13,** 13162–13166 (2011).
25. Lauwaet, K. *et al.* Resolving all atoms of an alkali halide via nanomodulation of the thin NaCl film surface using the Au(111) reconstruction. *Phys. Rev. B* **85,** 245440 (2012).
26. Hebenstreit, W. *et al.* Atomic resolution by STM on ultra-thin films of alkali halides: Experiment and local density calculations. *Surf. Sci.* **424,** L321–L328 (1999).
27. Cabrera-Sanfelix, P., Arnau, A., Darling, G. R. & Sanchez-Portal, D. Water adsorption and diffusion on NaCl(100). *J. Phys. Chem. B* **110,** 24559–24564 (2006).
28. Yang, Y., Meng, S. & Wang, E. G. Water adsorption on a NaCl(001) surface: A density functional theory study. *Phys. Rev. B* **74,** 245409 (2006).
29. Ho, W. Single-molecule chemistry. *J. Chem. Phys.* **117,** 11033–11061 (2002).
30. Martínez, J. I., Abad, E., González, C., Flores, F. & Ortega, J. Improvement of scanning tunneling microscopy resolution with H-sensitized tips. *Phys. Rev. Lett.* **108,** 246102 (2012).
31. Nørskov, J. K. Chemisorption on metal surfaces. *Rep. Prog. Phys.* **53,** 1253–1295 (1990).
32. Perrin, M. L. *et al.* Large tunable image-charge effects in single-molecule junctions. *Nature Nanotech.* **8,** 282–287 (2013).
33. Sautet, P. & Joachim, C. Calculation of the benzene on rhodium STM images. *Chem. Phys. Lett.* **185,** 23–30 (1991).
34. Lawton, T. J., Carrasco, J., Baber, A. E., Michaelides, A. & Sykes, E. C. H. Visualization of hydrogen bonding and associated chirality in methanol hexamers. *Phys. Rev. Lett.* **107,** 256101 (2011).
35. Horcas, I. *et al.* WSXM: A software for scanning probe microscopy and a tool for nanotechnology. *Rev. Sci. Instrum.* **78,** 013705 (2007).
36. Klimeš, J., Bowler, D. R. & Michaelides, A. Van der Waals density functionals applied to solids. *Phys. Rev. B* **83,** 195131 (2011).
37. Kresse, G. & Hafner, J. Ab initio molecular dynamics for liquid metals. *Phys. Rev. B* **47,** 558–561 (1993).
38. Kresse, G. & Furthmüller, J. Efficient iterative schemes for *ab initio* total-energy calculations using a plane-wave basis set. *Phys. Rev. B* **54,** 11169–11186 (1996).
39. Kresse, G. & Joubert, D. From ultrasoft pseudopotentials to the projector augmented-wave method. *Phys. Rev. B* **59,** 1758–1775 (1999).
40. Jonsson, H. *et al. Classical and Quantum Dynamics in Condensed Phase Simulations* Ch. 8 (World Scientific, 1998).

Acknowledgements

Author contributions

Y.J. and E.W. designed and supervised the project. J.G., X.M. and Y.J. performed the STM measurements. J.C., X-Z.L. and E.W. carried out the DFT calculations. J.G., X.M., J.C., J.P., X-Z.L., L.X., E.W. and Y.J. analysed the data. J.S. contributed to the STM programming. J-R.S. contributed to the interpretation of the data. Y.J. wrote the manuscript with J.G., X.M., J.C., J.P., X-Z.L. L.X. and E.W. The manuscript reflects the contributions of all authors.

Additional information

Supplementary information is available in the online version of the paper. Reprints and permissions information is available online at www.nature.com/reprints. Correspondence and requests for materials should be addressed to E.W. or Y.J.

Competing financial interests

The authors declare no competing financial interests.